Research Article

Artificial self-sufficient cytochrome P450 containing multiple auxiliary proteins demonstrates improved monooxygenase activity

Tomoaki Haga[1]

Hidehiko Hirakawa[1,2]

Teruyuki Nagamune[1]

[1]Department of Chemistry and Biotechnology, School of Engineering, The University of Tokyo, Tokyo, Japan

[2]Current address: Faculty of Life and Environmental Sciences, University of Tsukuba, 1-1-1 Tennodai, Tsukuba, Ibaraki 305-8572, Japan

Correspondence: Prof. Hidehiko Hirakawa, Faculty of Life and Environmental Sciences, University of Tsukuba, 1-1-1 Tennodai, Tsukuba, Ibaraki 305-8572, Japan

E-mail: hirakawa.hidehiko.ge@u.tsukuba.ac.jp

Keywords: artificial assembly; cytochrome P450; electron transfer; multienzyme complex; self-sufficient

Abbreviations: cyt*c*, cytochrome *c*; **ET,** electron transfer; **HS-P450cam^{3+},** substrate-bound high-spin P450cam; **P450,** cytochrome P450 monooxygenase; **LS-P450cam^{3+},** low-spin open state of P450cam; **P450cam,** a cytochrome P450 monooxygenase from Pseudomonas putida; **PCNA,** proliferating cell nuclear antigen; **PdR,** putidaredoxin

reductase; **PdX,** putidaredoxin; **PUPPET,** PCNA-united protein complex of P450 and electron transfer-related proteins; **SO-P450cam^{3+},** ferric superoxide P450cam

Abstract

Most bacterial cytochrome P450 monooxygenases (P450s) do not work alone because their active species is generated by two electrons supplied through two separate auxiliary proteins. Artificial "self-sufficient" P450s, in which one molecule each of the two auxiliary proteins is arranged close to the P450s, have been developed but have not achieved the maximum catalytic turnover numbers of the P450s. In this study, the *Pseudomonas putida* P450 (P450cam) was assembled with multiple molecules of its auxiliary proteins, putidaredoxin (PdX) and putidaredoxin reductase (PdR), by fusion to a heterotrimeric protein. In the assembled P450cam containing one PdX and one PdR, kinetic analysis revealed that the catalytic cycle of P450cam was suspended twice awaiting the reduction of PdX by PdR. An increase in the number of PdR molecules stimulated the PdX reduction process. Assembly with two PdXs allowed one PdX to be reduced during the binding of the other PdX to P450cam for the first electron transfer, eliminating one waiting step. Finally, P450cam assembled with two PdXs and three PdRs showed 92% of the maximum activity of free P450cam. Therefore, assembly with multiple molecules of auxiliary proteins will facilitate in vitro biotechnological applications of the P450s.

1 Introduction

Many enzymes interact with auxiliary proteins to achieve their catalytic activities. Post-translational modification [1] and allosteric conformational change [2,3] triggered by auxiliary proteins result in lasting activation of enzymes after or during interaction with the auxiliary proteins. Electron or substrate uptake/release by auxiliary proteins [4,5] is required for each catalytic cycle of some enzymes, and thus such enzymes require continual interactions with the refreshed auxiliary proteins. These enzymes can demonstrate their maximum activities when the refreshed auxiliary proteins are present in large excess. In nature, some enzymes also have multidomain structures in which auxiliary protein domains play a role in electron or substrate uptake/release [6–9], and thus these enzymes exhibit their catalytic activity without separate auxiliary proteins.

Cytochrome P450 monooxygenases (P450s) accept electrons for generation of active species [10], and catalyze regio- and stereoselective oxidations of non-activated C-H bonds [11] to produce diverse natural compounds [12]. Bacterial P450s, which are soluble proteins and generally have high catalytic turnover numbers compared with eukaryotic P450s [13], have been explored for chemical synthesis [14,15]. Recently, Bernhardt's group demonstrated that bacterial P450s are able to produce valuable compounds [16–18].

Generally, bacterial P450s accept two electrons, one at a time, from separate electron transfer (ET) proteins such as ferredoxin and flavodoxin [10]. There are also a few cases of naturally occurring fusions to redox domains [19]. In the typical case, the ET

proteins need to dissociate from the P450s and then be regenerated by their specific reductases. Accordingly, the interactions between the P450s and their specific ET proteins are weak, and micromolar concentrations of ET proteins are necessary for the P450s to show their maximal activity [20,21]. This requirement hinders practical applications of the P450s. To overcome this inconvenience, artificial "self-sufficient" P450s, in which redox proteins are arranged near a P450 moiety and supply electrons to it intramolecularly, have been developed [22,23], and chimeric constructs containing non-natural redox proteins have increased the versatility of bacterial P450s [24–26].

We previously reported artificial assembly of a bacterial P450 and its redox proteins using a *Sulfolobus solfataricus* proliferating cell nuclear antigen (PCNA) [27]. The PCNA consists of three distinct subunits, PCNA1, PCNA2 and PCNA3, which can be separately expressed as monomeric proteins [28]. Fusion to the PCNA subunits assembles P450cam, putidaredoxin (PdX) and putidaredoxin reductase (PdR), which are components of the camphor monooxygenase system from *Pseudomonas putida*, to form a protein complex containing one molecule each of P450cam, PdX and PdR (PCNA-united protein complex of P450 and ET-related proteins, PUPPET). PUPPET, in which electrons are efficiently donated to P450cam from PdR through PdX, demonstrated a much higher monooxygenase activity than free P450cam in the presence of equimolar PdX and PdR. Optimization of the peptide linker connecting a PCNA subunit and PdX improved the monooxygenase activity of PUPPET but did not achieve the maximum turnover number of P450cam [29], suggesting that the behavior of PdX dominates catalysis in PUPPET. Thus,

the catalytic activity of PUPPET could be further increased by improvement of the electron donation process from PdR to P450cam. Recently, Schulz et al. reported artificial reassembly of a natural fusion P450 from *Bacillus megaterium* [30], and revealed that the assembly with multiple redox domains enhanced the catalysis by the heme domain.

In this study, we evaluated the kinetics of the P450cam-catalyzed monooxygenase reaction with various numbers of the two auxiliary proteins (i.e. PdR and PdX) in PUPPET on the monooxygenase activity. Free P450cam can successively accept electrons from reduced PdX (PdX^{red}) when the concentration of PdX^{red} is sufficiently higher than the dissociation constant of P450cam. In contrast, in PUPPET containing only one PdX molecule, P450cam must wait for PdX reduction twice in each catalytic cycle. We show that increasing the number of PdR moieties enhanced the reduction and thus shortened the waiting times, increasing the monooxygenase activity of PUPPET. Moreover, in PUPPET containing two molecules of PdX, one PdX is reduced by PdR during the first ET process to P450cam from the other PdX, thus removing a waiting step. Eventually, 92% of the maximal activity of free P450cam was achieved by PUPPET containing two PdXs and three PdRs. Therefore, PCNA-mediated assembly with multiple copies of redox proteins will facilitate in vitro biotechnological applications of bacterial P450s.

2 Materials and methods

2.1 Preparation of PUPPET

The G108C variant of PCNA1 ($PCNA1_{G108C}$), L171C variant of PCNA2 ($PCNA2_{L171C}$), and R112C/T180C variant of PCNA3 ($PCNA3_{R112C/T180C}$) fused to PdR, PdX and/or P450cam (Fig. S1) were prepared as described in Supporting information. A $PCNA1_{G108C}$ fusion protein was mixed with one-equivalent of a $PCNA2_{L171C}$ fusion protein and 1.05-equivalents of a $PCNA3_{R112C/T180C}$ fusion protein and then loaded onto a HiTrap desalting

column (GE Healthcare, Little Chalfont, Buckinghamshire, UK) pre-equilibrated with Buffer A (50 mM potassium phosphate buffer, pH 7.4, containing 150 mM KCl and 5 mM D-camphor (Wako Pure Chemical Industries, Osaka, Japan)). The eluted mixture was incubated in the presence of 10 mM glutathione disulfide (Wako Pure Chemical Industries) at 4°C for 24 h, and then subjected to size-exclusion chromatography on a Superdex 200 Increase 10/300 GL column (1.0 × 30 cm; GE Healthcare) in Buffer A. The resulting PUPPETs containing *m* molecules of PdR, *n* molecules of PdX, and one molecule of P450cam, were named in the style R^mX^nC (Fig. 1). Complexes that did not contain P450cam (R^mX^n) were prepared as described above, except that D-camphor was not added into the buffers.

2.2. UV-vis spectral change of P450cam dependent on the numbers of PdR and PdX molecules in PUPPET

Equimolar mixtures of a $PCNA1_{G108C}$ fusion protein, a $PCNA2_{L171C}$ fusion protein and a $PCNA3_{R112C/T180C}$ protein fused to P450cam were incubated in Buffer A with 10 mM glutathione disulfide at 4°C for 24 h. UV-vis spectra of the equimolar mixtures were measured, using incubated equimolar mixtures of the $PCNA1_{G108C}$ fusion protein, $PCNA2_{L171C}$ fusion protein and $PCNA3_{R112C/T180C}$ as the reference. Then, difference spectra were obtained by subtracting the spectrum of P450cam from the observed spectra.

Eq. 1 and Eq. 2 were used to analyze the effect of the numbers of PdR and PdX molecules on the spectral change of P450cam in PUPPET. The PdX^{ox}-bound P450cam is in the low-spin open state [31,32] and has a Soret peak around 418 nm [33]. In the model, binding of oxidized PdX (PdX^{ox}) to PdR and P450cam is reversible (Model S1 in Supporting information).

$$\frac{1}{\Delta\Delta\mathrm{Abs}(\mathrm{R}^m\mathrm{X}^1\mathrm{C})} = \frac{1}{\Delta\Delta\mathrm{Abs}_{\max}}\left(1 + \frac{1}{K_1} + \frac{mK_2}{K_1}\right) \quad (1)$$

$$\frac{1}{\Delta\Delta\mathrm{Abs}(\mathrm{R}^{m}\mathrm{X}^{2}\mathrm{C})} = \frac{1}{\Delta\Delta\mathrm{Abs}_{\max}}\left(1 + \frac{1}{2K_1} + \frac{mK_2(1+(m-1)K_2)}{2K_1(1+mK_2)}\right) \quad (2)$$

where $\Delta\Delta\mathrm{Abs}(\mathrm{R}^{m}\mathrm{X}^{n}\mathrm{C})$ is the difference in absorbance between 392 nm and 418 nm in the difference spectra, and $\Delta\Delta\mathrm{Abs}_{\max}$ is the difference when P450cam completely binds to $\mathrm{PdX}^{\mathrm{ox}}$. K_1 and K_2 are equilibrium constants for the binding of $\mathrm{PdX}^{\mathrm{ox}}$ to substrate-bound high-spin P450cam (HS-$\mathrm{P450cam}^{3+}$) and of $\mathrm{PdX}^{\mathrm{ox}}$ to PdR, respectively (Figs. 2D and 2E). The $\Delta\Delta\mathrm{Abs}_{\max}$ and K_1 values were estimated from the observed $\Delta\Delta\mathrm{Abs}(\mathrm{R}^{0}\mathrm{X}^{1}\mathrm{C})$ and $\Delta\Delta\mathrm{Abs}(\mathrm{R}^{0}\mathrm{X}^{2}\mathrm{C})$ using Eqs. 1 and 2. The K_2 value was estimated from the observed $\Delta\Delta\mathrm{Abs}(\mathrm{R}^{m}\mathrm{X}^{1}\mathrm{C})$ by linear fitting to Eq. 1 with the $\Delta\Delta\mathrm{Abs}_{\max}$ and K_1 values. The fitting was conducted using GraphPad Prism 7.

2.3. Enzyme assays

Potassium ferricyanide reduction activity was evaluated by measuring the decrease of its absorption at 420 nm ($\Delta\varepsilon_{420}$ = 1.02 mM^{-1} cm^{-1}). The reaction was performed in 50 mM potassium phosphate buffer, pH 7.4, containing 150 mM KCl, 1 mM potassium ferricyanide (Kokusan Chemical Works, Tokyo, Japan), 500 μM NADH (Wako Pure Chemical Industries), and 1 nM PUPPET. Cytochrome *c* (cyt*c*) reduction rate was determined by measuring its absorption change at 550 nm ($\Delta\varepsilon_{550}$ = 21.1 mM^{-1} cm^{-1}). The reaction was performed in 50 mM potassium phosphate buffer, pH 7.4, containing 150 mM KCl, 5–200 μM equine heart cyt*c* (Sigma-Aldrich, St. Louis, MO, USA), 500 μM NADH, and 1 nM $\mathrm{R}^{m}\mathrm{X}^{n}\mathrm{C}$ or $\mathrm{R}^{m}\mathrm{X}^{n}$. Monooxygenase activity of PUPPET was evaluated from the NADH consumption rate and the coupling efficiency (see section 2.4). The reaction was performed in 50 mM potassium phosphate buffer, pH 7.4, containing 150 mM KCl, 1 mM D-camphor, 100 μM NADH and 20 nM PUPPET. The NADH consumption rate was calculated from the initial decrease rate in absorption at 340 nm ($\Delta\varepsilon_{340}$ = 6.22 mM^{-1} cm^{-1}). All assays were conducted at 25°C.

2.4. Coupling efficiency

The coupling of D-camphor consumption to NADH consumption was measured in 50 mM potassium phosphate buffer, pH 7.4, containing 150 mM KCl, 1 mM D-camphor, 500 μM NADH and 20 nM PUPPET at 25°C for 1 h. The reaction mixture contained the excess of D-camphor to avoid the uncoupled NADH consumption that is caused by autoxidation of PdR and PdX in the absence of D-camphor. After the reaction, D-camphor was immediately extracted twice with 500 μL dichloromethane containing 400 μM 3-*endo*-bromocamphor (Tokyo Chemical Industry, Tokyo, Japan). After washing with saturated NaCl solution, the extract was dried with anhydrous sodium sulfate (Wako Pure Chemical Industries). The dried extract was concentrated under a N_2 flow and then analyzed by gas chromatography (Hewlett-Packard 6850 equipped with a flame ionization detector and a HP-1 column). NADH consumption was estimated by measuring the absorption at 340 nm of the water layer after the extraction. The coupling efficiency was determined by dividing the amount of D-camphor consumed by the amount of NADH consumed.

2.5. Steady-state kinetic analysis of cytochrome *c* reduction

We assumed that the low-spin open state of P450cam (LS-P450cam^{3+}) binds to PdX^{ox} and reduced PdX (PdX^{red}) (Fig. 3A), cyt*c* reduction by PdX^{red} [34] is much faster than PdX reduction by PdR [35], and auto-oxidations of PdR and PdX as well as the intercomplex ET between PdR and PdX are negligible. PdR, which has two forms that transfer an electron to PdX^{ox} [36]—the reduced form and the semiquinone form—was simply assumed to be an enzyme that converts PdX^{ox} to PdX^{red} without distinction between the two forms because the reaction rates were evaluated in the steady-state.

Thus, kinetic constants (V_{max} and V_{max}/K_m) for the cyt*c* reduction reaction by R^{m}X^{1}C are represented by the following equations (Model S2 in Supporting information):

$$V_{\max} = k_{\mathrm{cyt}c}{}^{\mathrm{R}m\mathrm{X}1\mathrm{C}}[\mathrm{R}^m\mathrm{X}^1\mathrm{C}] = \frac{1}{\frac{k_{-2}+k_3}{mk_2k_3}\left(1+\frac{k_{-1}}{k_1}\right)+\frac{1}{k_3}}[\mathrm{R}^m\mathrm{X}^1\mathrm{C}] \quad (3)$$

$$\frac{V_{\max}}{K_{\mathrm{m}}} = \frac{k_4k_5}{(k_{-4}+k_5)\left(1+\frac{k_6}{k_{-6}}\right)}[\mathrm{R}^m\mathrm{X}^1\mathrm{C}] \quad (4)$$

The constants in the equations are rate constants of dissociation of $\mathrm{PdX^{ox}}$ from LS-$\mathrm{P450cam^{3+}}$ (k_1, state II to I), binding of $\mathrm{PdX^{ox}}$ to LS-$\mathrm{P450cam^{3+}}$ (k_{-1}, state I to II), binding of $\mathrm{PdX^{ox}}$ to PdR (k_2, state I to III), dissociation of $\mathrm{PdX^{ox}}$ from PdR (k_{-2}, state III to I), a transition from the $\mathrm{PdX^{ox}}$-PdR complex to free $\mathrm{PdX^{red}}$ (k_3, state III to IV), binding of $\mathrm{PdX^{red}}$ to cyt*c* (k_4, state IV to VI), dissociation of $\mathrm{PdX^{red}}$ from cyt*c* (k_{-4}, state VI to IV), reduction of cyt*c* by $\mathrm{PdX^{red}}$ (k_5, state VI to I), binding of $\mathrm{PdX^{red}}$ to LS-$\mathrm{P450cam^{3+}}$ (k_6, state IV to V), and dissociation of $\mathrm{PdX^{red}}$ from LS-$\mathrm{P450cam^{3+}}$ (k_{-6}, state V to IV) as indicated in Fig. 3A.

The kinetic constants for the reaction by $\mathrm{R}^m\mathrm{X}^1$ are given by:

$$V_{\max} = k_{\mathrm{cyt}c}{}^{\mathrm{R}m\mathrm{X}1}[\mathrm{R}^m\mathrm{X}^1] = \frac{1}{\frac{k_{-2}+k_3}{mk_2k_3}+\frac{1}{k_3}}[\mathrm{R}^m\mathrm{X}^1] \quad (5)$$

$$\frac{V_{\max}}{K_{\mathrm{m}}} = \frac{k_4k_5}{k_{-4}+k_5}[\mathrm{R}^m\mathrm{X}^1] \quad (6)$$

The kinetic constants for the reaction by $\mathrm{R}^m\mathrm{X}^2\mathrm{C}$ and $\mathrm{R}^m\mathrm{X}^2$ were derived, assuming the following. When the cyt*c* reduction rate is saturated with respect to the cyt*c* concentration, the presence of $\mathrm{PdX^{red}}$ is negligible owing to exclusive and immediate complexation with cyt*c*. In contrast, when the concentration of cyt*c* is much lower than K_{m}, at least one molecule of PdX remains in the reduced state owing to slow electron efflux (Model S3 in Supporting information). Thus, the kinetic constants for the reaction by $\mathrm{R}^m\mathrm{X}^2\mathrm{C}$ are given by:

$$V_{\max} = \frac{1+\frac{(m-1)k_2}{(k_{-2}+k_3)\left(1+\frac{k_{-1}}{k_1}\right)}}{\frac{k_{-2}+k_3}{2mk_2k_3}\left(1+\frac{1}{1+\frac{k_1}{k_{-1}}}\right)+\frac{(m-1)k_2}{2k_3(k_{-2}+k_3)\left(1+\frac{k_{-1}}{k_1}\right)}+\frac{1}{k_3}}[\mathrm{R}^m\mathrm{X}^2\mathrm{C}] \quad (7)$$

$$\frac{V_{\max}}{K_{\mathrm{m}}} = \frac{2k_4k_5\left(1+\frac{k_6}{k_{-6}}\right)}{(k_{-4}+k_5)\left(1+\frac{2k_6}{k_{-6}}\right)}[\mathrm{R}^m\mathrm{X}^2\mathrm{C}] \quad (8)$$

and those for the reaction by $\mathrm{R}^m\mathrm{X}^2$ are given by:

$$V_{\max} = \frac{1 + \frac{(m-1)k_2}{k_{-2}+k_3}}{\frac{k_{-2}+k_3}{2mk_2k_3} + \frac{(m-1)k_2}{2k_3(k_{-2}+k_3)} + \frac{1}{k_3}} [\mathrm{R}^m\mathrm{X}^2] \quad (9)$$

$$\frac{V_{\max}}{K_{\mathrm{m}}} = \frac{2k_4k_5}{k_{-4}+k_5} [\mathrm{R}^m\mathrm{X}^2] \quad (10)$$

2.6. Kinetic model of the monooxygenase reaction

PdX in R^{m}X^{1}C is reduced by PdR after transferring an electron to P450cam, and thus the reaction cycle of R^{m}X^{1}C is illustrated in Fig. 4A. The rate constant of the monooxygenase activity, k^{RmX1C}, is expressed as follows (Model S4 in Supporting information):

$$\frac{1}{k^{\mathrm{RmX1C}}} = \frac{k_{-2}+k_3}{mk_2k_3}\left(2 + \frac{k_{-1}}{k_1} + \frac{k_{-9}}{k_9}\right) + \frac{2}{k_3} + \frac{k_{-7}+k_8}{k_7k_8} + \frac{1}{k_8} + \frac{1}{k_9} + \frac{k_{-10}+k_{11}}{k_{10}k_{11}} + \frac{1}{k_{11}} + \frac{1}{k_1} \quad (11)$$

The constants in Eq. 11 are rate constants of binding of PdX$^{\mathrm{red}}$ to HS-P450cam^{3+} (k_7, state (**3**) to (**4**)), dissociation of PdX$^{\mathrm{red}}$ from HS-P450cam^{3+} (k_{-7}, state (**4**) to (**3**)), a transition from the HS-P450cam^{3+}/PdX$^{\mathrm{red}}$ complex to the ferric superoxide P450cam (SO-P450cam^{3+})/PdX$^{\mathrm{ox}}$ complex (k_8, state (**4**) to (**5**)), dissociation of PdX$^{\mathrm{ox}}$ from SO-P450cam^{3+} (k_9, state (**5**) to (**6**)), binding of PdX$^{\mathrm{ox}}$ to SO-P450cam^{3+} (k_{-9}, state (**6**) to (**5**)), binding of PdX$^{\mathrm{red}}$ to SO-P450cam^{3+} (k_{10}, state (**7**) to (**8**)), dissociation of PdX$^{\mathrm{red}}$ from SO-P450cam^{3+} (k_{-10}, state (**8**) to (**7**)), and transition from SO-P450cam^{3+}/PdX$^{\mathrm{red}}$ to the LS-P450cam^{3+}/PdX$^{\mathrm{ox}}$ complex (k_{11}, state (**8**) to (**1**)).

If the binding of PdX$^{\mathrm{red}}$ to P450cam in R^{m}X^{1}C is much faster than the other processes in the catalytic cycle of P450cam (k_7 >> k_{-7}, k_8; k_{10} >> k_{-10}, k_{11}), and PdX$^{\mathrm{ox}}$ interacts with SO-P450cam^{3+} as strongly as with HS-P450cam^{3+}, Eq. 11 can be simplified to:

$$\frac{1}{k^{\mathrm{RmX1C}}} = 2\left(\frac{k_{-2}+k_3}{mk_2k_3}\left(1 + \frac{k_{-1}}{k_1}\right) + \frac{1}{k_3}\right) + \frac{1}{k_8} + \frac{1}{k_9} + \frac{1}{k_{11}} + \frac{1}{k_1} \quad (12)$$

The maximum catalytic turnover of P450cam is given (Model S5 in Supporting information) by:

$$\frac{1}{k_{\mathrm{cat}}^{\mathrm{P450cam}}} = \frac{1}{k_8} + \frac{1}{k_9} + \frac{1}{k_{11}} + \frac{1}{k_1} \quad (13)$$

Therefore,

$$\frac{1}{k^{\mathrm{R}m\mathrm{X1C}}} = \frac{2}{k_{\mathrm{red}}{}^{\mathrm{R}m\mathrm{X1C}}} + \frac{1}{k_{\mathrm{cat}}{}^{\mathrm{P450cam}}} \quad (14)$$

Here, $k_{\mathrm{red}}{}^{\mathrm{R}m\mathrm{X1C}}$ is a rate constant for PdX reduction by PdR, and is identical to the turnover number of R^{m}X^{1}C for the cyt*c* reduction, $k_{\mathrm{cyt}c}{}^{\mathrm{R}m\mathrm{X1C}}$ (Eq. 3), owing to the much faster reduction of cyt*c* by PdX$^{\mathrm{red}}$ than that of PdX$^{\mathrm{ox}}$ by PdR [34].

The reaction cycle of R^{m}X^{2}C is illustrated in Fig. 4B. One PdX can be reduced by PdR during the first ET from the other PdX to P450cam and the oxygen binding process ((**4**) to (**5**) in Fig. 4B). The rate constant of the monooxygenase reaction by R^{m}X^{2}C, $k^{\mathrm{R}m\mathrm{X2C}}$, is expressed as follows (Model S6 in Supporting information):

$$\frac{1}{k^{\mathrm{R}m\mathrm{X2C}}} = \frac{k_{-2}+k_3}{mk_2k_3} + \frac{1}{k_3} + \frac{k_{-7}+k_8}{k_7k_8}\left(1+\frac{k_{-1}}{k_1}\right) + \frac{1}{k_8} + \frac{1}{k_9} + \frac{k_{-10}+k_{11}}{k_{10}k_{11}}\left(1+\frac{k_{-9}}{k_9}\right) + \frac{1}{k_{11}} + \frac{1}{k_1} \quad (15)$$

When the bindings of PdX$^{\mathrm{red}}$ to P450cam in R^{m}X^{2}C are much faster than the other processes (k_7 >> k_{-7}, k_8; k_{10} >> k_{-10}, k_{11}), Eq. 15 can be simplified to:

$$\frac{1}{k^{\mathrm{R}m\mathrm{X2C}}} = \frac{k_{-2}+k_3}{mk_2k_3} + \frac{1}{k_3} + \frac{1}{k_8} + \frac{1}{k_9} + \frac{1}{k_{11}} + \frac{1}{k_1} = \frac{1}{k_{\mathrm{red}}{}^{\mathrm{R}m\mathrm{X1}}} + \frac{1}{k_{\mathrm{cat}}{}^{\mathrm{P450cam}}} \quad (16)$$

where $k_{\mathrm{red}}{}^{\mathrm{R}m\mathrm{X1}}$ is the rate constant for PdX reduction by PdR in R^{m}X^1, and is identical to the turnover number of R^{m}X^1 for cyt*c* reduction, $k_{\mathrm{cyt}c}{}^{\mathrm{R}m\mathrm{X1}}$ (Eq. 5). The above equations are derived under the assumption that auto-oxidations of PdR and PdX and intercomplex ET from PdR to PdX and PdX to P450cam are negligible.

3 Results

3.1. PCNA fusion proteins to generate PUPPETs containing multiple molecules of PdX and PdR

To prepare PUPPETs containing multiple copies of PdX and PdR, PdR was fused to the N-termini of the G108C variant of PCNA1 (PCNA1$_{\mathrm{G108C}}$), the L171C variant of PCNA2 (PCNA2$_{\mathrm{L171C}}$) and the R112C/T180C of PCNA3 (PCNA3$_{\mathrm{R112C/T180C}}$), PdX was fused to the C-

termini of PCNA1$_{G108C}$ and PCNA2$_{L171C}$ via an optimized peptide linker [29], and P450cam was fused to the C-terminus of PCNA3$_{R112C/T180C}$ (Fig. S1). Newly constructed fusion proteins, PCNA1$_{G108C}$-PdX, PdR-PCNA2$_{L171C}$, PdR-PCNA2$_{L171C}$-PdX and PdR-PCNA3$_{R112C/T180C}$-P450cam, showed characteristic UV-vis spectra derived from their functional moieties (Fig. S2), and showed similar functions to the free counterparts of the fusion proteins: PdR-fused proteins showed similar potassium ferricyanide reduction activity to free PdR (Table S1); PdX-fused proteins facilitated electron flow to P450cam from PdR to the same extent as free PdX (Table S2); and PdR-PCNA3$_{R112C/T180C}$-P450cam as well as PCNA3$_{R112C/T180C}$-P450cam showed similar NADH consumption activity to free P450cam in the presence of free PdX and PdR (Table S3).

3.2. Spectral analysis of PUPPET

PUPPETs containing multiple molecules of PdX and PdR (R^mX^nC: *m*, the number of PdR molecules; *n*, the number of PdX molecules) were prepared by mixing three PCNA subunit fusion proteins (Fig. 1) with subsequent intersubunit disulfide bond formation [37] (Fig. S3), conditions for which were optimized in advance (Fig. S4). Each PUPPET showed a slightly different UV-vis spectrum from a linear combination of the spectra of the component fusion proteins in the region 350 to 450 nm (Figs. 2A and S5). The spectrum of each complex lacking P450cam, R^mX^n, was identical to that of a linear combination of the component proteins (Fig. S6). This result indicates that the spectral change of PUPPET corresponds to a change of a Soret peak of P450cam in PUPPET, and thus the spectra of P450cam in R^mX^nC were measured using R^mX^n as a reference. The difference between absorbance at 392 nm and 418 nm in the difference spectra, ΔΔAbs, increased with an increase in the number of PdX molecules, but decreased with an increase in the number of PdR molecules (Figs. 2B and 2C).

The spectral change of P450cam in PUPPET was analyzed by a steady-state competition model of interactions of PdX^{ox} with P450cam and PdR in PUPPET (Figs. 2D and 2E). The equilibrium constant for binding of PdX^{ox} to P450cam, K_1, in PUPPETs was determined to be 1.1 from the observed spectral changes observed in R^0X^1C and R^0X^2C using Eqs. 1 and 2. The equilibrium constant for binding of PdX^{ox} to PdR, K_2, in PUPPETs was calculated to be 1.3 from the observed spectral changes in R^mX^1C using Eq. 1. The calculated ΔΔAbs values of R^1X^2C, R^2X^2C and R^3X^2C were similar to the observed values (Fig. 2F). The binding states of PdX^{ox} in PUPPETs were quantitatively determined as shown in Table S4.

3.3. Effect of the numbers of PdX and PdR molecules on reduction of PdX

The cyt*c* reduction reaction by R^mX^nC and R^mX^n apparently followed Michaelis-Menten kinetics (Fig. S7). The kinetic parameters were affected by the composition of PUPPET (Table S5): the V_{max} values increased with an increase in the numbers of PdX and PdR. The V_{max}/K_m values were exclusively dependent upon the number of PdX molecules. Furthermore, the V_{max} and V_{max}/K_m values for R^mX^nC were lower than those for R^mX^n.

We developed kinetic models of the cyt*c* reduction reaction (Fig. 3 and Section 2.5). In the models, PUPPET is proposed to change its state during the cyt*c* reduction process as follows (Fig. 3A): PdX^{ox} binds to PdR (state I to III), PdX^{red} dissociates from PdR after the reduction (state III to IV), cyt*c* binds to PdX^{red} (state IV to VI), and, finally, reduced cyt*c* is released (state VI to I). LS-$P450cam^{3+}$ was assumed to interact with PdX^{ox} (state I to II) and PdX^{red} (state IV to V). Our model reproduced the observed kinetic parameters well (Table S5). As observed (Table S5), the V_{max}/K_m values of PUPPET are suggested to be independent of PdR but dependent on PdX and P450cam (Eqs. 4, 6, 8 and 10) due to the interaction between PdX^{red} and LS-$P450cam^{3+}$. The calculated V_{max} values were similar to the observed values. It is worth noting that the calculated V_{max} values of R^mX^2 were quite

similar to those observed, even though $(k_{-2}+k_3)/k_2$ and k_3 values that were determined from the observed V_{max} values of R^mX^1 were used to calculate the values. The calculated V_{max} values of R^mX^1C and R^mX^2C were also similar to the observed values. The value of k_{-1}/k_1 was determined to be 0.96.

3.4. Effect of the numbers of PdX and PdR molecules on monooxygenase activity

PUPPETs containing multiple PdX and/or PdR molecules demonstrated improved activities compared with the PUPPET containing one PdX and one PdR with high coupling efficiency (Table 1 and Fig. S8). The activity simply increased with an increase in the numbers of PdX and PdR molecules. R^3X^2C showed 92% of the maximum activity of free P450cam (Fig. S9).

The monooxygenase activity of PUPPET may be predicted from the catalytic turnover number of free P450cam and the cyt*c* reduction activity of PUPPET. PdX can carry one electron at once, and can be re-reduced after an ET to P450cam in R^mX^1C (Fig. 4A). The complete catalytic cycle of P450s contains two ET processes, and thus the cycle of P450cam in R^mX^1C needs to wait twice for the PdX reduction process. If the progressive bindings of PdX^{red} to HS-$P450cam^{3+}$ (state (**3**) to (**4**) in Fig. 4A) and SO-$P450cam^{3+}$ (state (**7**) to (**8**) in Fig. 4A) are much faster than the other steps, and PdX^{ox} interacts with SO-$P450cam^{3+}$ as strongly as with HS-$P450cam^{3+}$ in R^mX^1C, the catalytic activity of R^mX^1C may simply be predicted from the reduction rate constant of PdX in R^mX^1C, which can be estimated from cyt*c* reduction activity, and the catalytic turnover number of P450cam (Eq. 14). Indeed, the calculated values of the monooxygenase activity of R^mX^1C were similar to the observed values (Table 1). Meanwhile, the monooxygenase activity of R^mX^2C may be predicted from the maximum turnover number of P450cam and the cyt*c* reduction activity of R^mX^1 (Eq. 16) under the assumption that a complex of PdX^{ox} and LS-$P450cam^{3+}$ would be retained during the PdX reduction after the release of product 5-exo-hydroxycamphor

from R^mX^2C (state (**1**) to (**1′**) in Fig. 4B). The calculated values of the monooxygenase activity of R^mX^2C are also similar to the observed values (Table 1).

4 Discussion

Multiple molecules of PdX and PdR were assembled with P450cam on the *S. solfataricus* PCNA ring. The PCNA can assemble up to six protein molecules without impairing their function [38]. Genetic fusion of a bacterial P450 and redox proteins also yields artificial self-sufficient P450s [22, 25, 26], in which the component proteins are not equivalently arranged, but artificial genetic fusion proteins composed of more than three proteins are difficult to express as fully active proteins in *E. coli*. Moreover, in contrast to artificial assemblies using a single self-assembling protein [30], the PCNA-mediated assembly in a stepwise fashion exclusively yields homogeneous complexes, and completely controls the numbers of PdX and PdR molecules. As reported recently [39], the interaction between PdX and P450cam was expected to affect the stability of PUPPETs without the disulfide bonds between the PCNA subunits, which affects their apparent turnover numbers, during the reaction. Thus, the disulfide bonds were introduce into PUPPETs under an optimized condition.

The assembly induced spectral change of P450cam, which was similar to that for ferric P450cam induced by PdX^{ox} [40], i.e., a red-shift in the Soret band from the high-spin closed conformation to the low-spin open conformation (Fig. S10). The change was suppressed by PdR, indicating that the ferric P450cam interacts with PdX^{ox} in PUPPET and the interaction competes with that between PdX^{ox} and PdR (Figs. 2D and 2E). This competition is reasonable because both PdR and P450cam recognize the surface region of PdX burying the [2Fe-2S] cluster [40,41]. Our competition model revealed that the presence of additional PdR and PdX moieties promoted the binding of PdX^{ox} to PdR (state iii/iv in Table S4), and could improve the apparent reduction rate of PdX.

In fact, the PdX reduction was stimulated by additional PdR and PdX. The cyt*c* reduction activity reflects the reduction of PdX by PdR in PUPPET for the following reasons: PdX^{red} can reduce cyt*c* much rapidly (>2000 s^{-1}) [34] compared with reduction of PdX by PdR [35] (k_5 >> k_3); direct reduction of cyt*c* by PdR and ET between PUPPET molecules are negligible at the concentrations of the proteins in the experiment (Fig. S7A); and the lower reduction potential of D-camphor-unbound P450cam (−340 mV) than of PdX (−239 mV) [42] hampers ET from PdX to P450cam in the absence of D-camphor. The consistency of our kinetic model with the acquired data (Table S5) validates that the reduction rate of PdX by PdR in PUPPET can be estimated from V_{max} of the cyt*c* reduction reaction (Fig. 3B and 3C).

The PdX reduction was inhibited by the binding of PdX^{ox} to LS-$P450cam^{3+}$, as suggested by comparison between cyt*c* reduction rates of R^mX^n and R^mX^nC (Table S5). The value of k_{-1}/k_1, which is a ratio of the association rate constant of PdX^{ox} with LS-$P450cam^{3+}$ to the dissociation rate constant, is similar to the value of K_1, which is the equilibrium constant of the transition from the closed conformation to the open conformation of P450cam on the binding of PdX^{ox} in the presence of substrate, though PdX^{ox} is reported to more strongly bind to LS-$P450cam^{3+}$ than HS-$P450cam^{3+}$ [43]. This suggests that LS-$P450cam^{3+}$ interacts with PdX^{ox} similarly to HS-$P450cam^{3+}$ in PUPPET. A complex of LS-$P450cam^{3+}$ and PdX^{ox} (state II in Fig. 3B) interferes with the complex formation of PdX^{ox} and PdR (state III in Fig. 3B), which dominates the reduction process of PdX.

Additional PdRs inhibit the binding of PdX^{ox} to LS-$P450cam^{3+}$ in PUPPET (i.e. lead to a decrease in the amount of state II), in addition to facilitating the binding of PdX^{ox} to PdR (i.e. increasing the amount of state III) (Table S5). These two events effectively enhanced the reduction of PdX in PUPPETs. Additional PdX can stimulate complex formation of LS-$P450cam^{3+}$ with PdX^{ox} as well as of PdR with PdX^{ox}. Furthermore, an alternative (i.e. a second) PdX^{ox} moiety cannot be trapped by P450cam in R^mX^2C (Fig. 3C),

and its presence therefore effectively facilitates the binding of PdX^{ox} to PdR in PUPPET. Thus, additional PdR and PdX molecules increase the proportion of the complex of PdR and PdX^{ox}, resulting in the enhancement of reduction of PdX.

The monooxygenase activity of PUPPET was effectively improved by additional PdX molecules because the catalytic cycle of P450cam in R^mX^2C would be suspended only once by waiting for PdX reduction (Fig. 4B) but that in R^mX^1C would be suspended twice (Fig. 4A). The first ET, whose rate (2.4×10^3 min^{-1}) is comparable to the monooxygenase activity of P450cam (2.3×10^3 min^{-1}) [44], is the rate-limiting step in P450cam catalysis. The rate is lower than the reduction rate of PdX in PUPPET (6.4×10^3 min^{-1}), which was estimated from V_{max} of cyt*c* reduction by R^1X^1. Therefore, an additional PdX (i.e. the second PdX molecule in the R^mX^2C PUPPET) should be reduced during the first ET (state (**4**) to (**5**) in Fig. 4B). After the dissociation of PdX^{ox} from SO-P450cam^{3+}, P450cam can immediately associate with the second PdX^{red} to accept the second electron (state (**7**) to (**8**) in Fig. 4B). The second ET rate, which had been determined to be 7.1×10^3 min^{-1} at 4°C [45], should be much faster than the turnover number of PdR in PdX reduction (1.6×10^4 min^{-1}) at 25°C [35]. Thus, in R^mX^2C, only the first PdX must be reduced by PdR once after the complete catalytic cycle of P450cam, and transfer the first electron in the next catalytic cycle. The reduction of the first PdX would be stimulated by additional PdR molecules in R^mX^2C, as in R^mX^1C.

Our kinetic models reveal that R^mX^1C and R^mX^2C never achieve the maximum catalytic turnover number of P450cam because the PdX reduction process suspends the catalytic cycle of P450cam. However, the parallel PdX reduction during the first ET in R^mX^2C raises the possibility of simultaneous reduction of two PdX molecules in R^mX^3C during the first ET (Fig. 4C). If two additional PdX molecules are reduced during binding of the first PdX to P450cam in PUPPET (state (**4**) to (**5**) in Fig. 4C), the second PdX^{red} can immediately bind to SO-P450cam^{3+} for the second ET, and the third PdX^{red} is available for

the first ET in the next catalytic cycle. As a result, $R^{m}X^{3}C$ would achieve the maximum catalytic turnover number of P450cam without waiting for PdX reduction. The turnover number of PdR in PdX reduction (1.6×10^{4} min^{-1}) [35] is much higher than the first ET rate (2.4×10^{3} min^{-1}), and one PdR reduced two PdXs at the rate of 5.0×10^{3} min^{-1} per PdX molecule in $R^{1}X^{2}$ (Table S5). Thus, a PUPPET containing one PdR and three PdXs, $R^{1}X^{3}C$, should demonstrate the same activity as free P450cam in saturated conditions. Unfortunately, PUPPETs containing three PdXs could not be prepared because the C-terminus of PdX is unavailable for fusion [23], and P450cam fused to PdX via PCNA3 was partially inactivated (Fig. S11). In other words, PUPPET with complete monooxygenase activities will be constructed using bacterial P450s and their redox partners where both termini are available for fusion to the PCNA subunits without loss of function.

Acknowledgement

This work was supported by the Hokuto Foundation for Bioscience and JSPS KAKENHI Grant Number JP18K04846. T.H. was supported by JSPS Research Fellowships for Young Scientists (25-9876).

Conflict of interest

The authors declare no financial or commercial conflict of interest.

5 References

[1] H. Ryšlavá, V. Doubnerová, D. Kavan, O. Vaněk, *J. Proteomics* **2013**, *92*, 80.

[2] J. M. Murphy, H. Farhan, P. A. Eyers, *Biochem. Soc. Trans.* **2017**, *45*, 537.

[3] L. K. Langeberg, J. D. Scott, *Nat. Rev. Mol. Cell Biol.* **2015**, *16*, 232.

[4] D. J. Ferraro, L. Gakhar, S. Ramaswamy, *Biochem. Biophys. Res. Commun*. **2005**, *338*, 175.

[5] S. W. White, J. Zheng, Y. -M. Zhang, C. O. Rock, *Annu. Rev. Biochem*. **2005**, *74*, 791.

[6] M. A. Fischbach, C. T. Walsh, *Chem. Rev.* **2006**, *106*, 3468.

[7] M. S. Patel, N. S. Nemeria, W. Furey, F. Jordan, *J. Biol. Chem.* **2014**, *289*, 16615.

[8] M. Nojiri, Y. Xie, T. Inoue, T. Yamamoto, H. Matsumura, K. Kataoka, Deligeer, K. Yamaguchi, Y. Kai, S. Suzuki, *Proc. Natl. Acad. Sci. U. S. A.* **2007**, *104*, 4315.

[9] H. Toyama, F. S. Mathews, O. Adachi, K. Matsushita, *Arch. Biochem. Biophys.* **2004**, *428*, 10.

[10] D. J. Cook, J. D. Finnigan, K. Cook, G. W. Black, S. J. Charnock, in *Advances in Protein Chemistry and Structural Biology*, Vol. 105 (Ed: C. Z. Christov), Elsevier Academic Press, San Diego, USA, **2016**, Ch. 5.

[11] P. R. Ortiz de Montellano, *Chem. Rev.* **2010**, *110*, 932.

[12] L. M. Podust, D. H. Sherman, *Nat. Prod. Rep.* **2012**, *29*, 1251.

[13] D. F. V. Lewis, P. Hlavica, *Biochim. Biophys. Acta-Bioenerg.* **2000**, *1460*, 353.

[14] H. M. Girvan, A. W. Munro, *Curr. Opin. Chem. Biol.* **2016**, *31*, 136.

[15] D. Schmitz, S. Janocha, F. M. Kiss, R. Bernhardt, *Biochim. Biophys. Acta-Proteins Proteomics* **2018**, *1866*, 11.

[16] T. T. B. Ly, A. Schifrin, B. D. Nguyen, R. Bernhardt, *J. Agric. Food Chem.* **2017**, *65*, 3891.

[17] M. Milhim, N. Putkaradze, A. Abdulmughni, F. Kern, P. Hartz, R. Bernhardt, *J. Biotechnol.* **2016**, *240*, 68.

[18] F. Kern, Y. Khatri, M. Litzenburger, R. Bernhardt, *Drug Metab. Dispos.* **2016**, *44*, 495.

[19] A. Ciaramella, D. Minerdi, G. Gilardi, *Rend. Fis. Acc. Lincei.* **2017**, *28*, S169.

[20] W. Yang, S. G. Bell, H. Wang, W. Zhou, N. Hoskins, A. Dale, M. Bartlam, L. -L. Wong, Z. Rao, *J. Biol. Chem.* **2010**, *285*, 27372.

[21] S. G. Bell, J. H. C. McMillan, J. A. Yorke, E. Kavanagh, E. O. D. Johnson, L. -L. Wong, *Chem. Commun.* **2012**, *48*, 11692.

[22] O. Sibbesen, J. J. De Voss, P. R. Ortiz de Montellano, *J. Biol. Chem.* **1996**, *271*, 22462.

[23] H. Hirakawa, N. Kamiya, T. Tanaka, T. Nagamune, *Protein Eng. Des. Sel.* **2007**, *20*, 453.

[24] R. Suzuki, H. Hirakawa, T. Nagamune, *Biotechnol. J.* **2014**, *9*, 1573.

[25] S. Negretti, A. R. H. Narayan, K. C. Chiou, P. M. Kells, J. L. Stachowski, D. A. Hansen, L. M. Podust, J. Montgomery, D. H. Sherman, *J. Am. Chem. Soc.* **2014**, *136*, 4901.

[26] J. K. Kulig, C. Spandolf, R. Hyde, A. C. Ruzzini, L. D. Eltis, G. Grönberg, M. A. Hayes, G. Grogan, *Bioorg. Med. Chem.* **2015**, *23*, 5603.

[27] H. Hirakawa, T. Nagamune, *ChemBioChem* **2010**, *11*, 1517.

[28] I. Dionne, R. K. Nookala, S. P. Jackson, A. J. Doherty, S. D. Bell, *Mol. Cell.* **2003**, *11*, 275.

[29] T. Haga, H. Hirakawa, T. Nagamune, *PLoS One* **2013**, *8*, e75114.

[30] S. Schulz, D. Schumacher, D. Raszkowski, M. Girhard, V. B. Urlacher, *Front. Bioeng. Biotechnol.* **2016**, *4*, 1.

[31] S. -H. Liou, M. Mahomed, Y. -T. Lee, D. B. Goodin, *J. Am. Chem. Soc.* **2016**, *138*, 10163.

[32] D. Batabyal, L. S. Richards, T. L. Poulos, *J. Am. Chem. Soc.* **2017**, *139*, 13193.

[33] M. Unno, J. F. Christian, D. E. Benson, N. C. Gerber, S. G. Sligar, P. M. Champion, *J. Am. Chem. Soc.* **1997**, *119*, 6614.

[34] P. W. Roome, J. A. Peterson, *Arch. Biochem. Biophys.* **1988**, *266*, 41.

[35] I. F. Sevrioukova, T. L. Poulos, *J. Biol. Chem.* **2002**, *277*, 25831.

[36] I. F. Sevrioukova, J. T. Hazzard, G. Tollin, T. L. Poulos, *Biochemistry* **2001**, *40*, 10592.

[37] H. Hirakawa, A. Kakitani, T. Nagamune, *Biotechnol. Bioeng.* **2013**, *110*, 1858.

[38] C. Y. Tan, H. Hirakawa, T. Nagamune, *Sci. Rep.* **2015**, *5*, 8648.

[39] F. Iwata, H. Hirakawa, T. Nagamune, *Biotechnol. J*. **2018**, 1700662.

[40] S. Tripathi, H. Li, T. L. Poulos, *Science* **2013**, *340*, 1227.

[41] I. F. Sevrioukova, T. L. Poulos, I. Y. Churbanova, *J. Biol. Chem.* **2010**, *285*, 13616.

[42] S. G. Sligar, I. C. Gunsalus, *Proc. Natl. Acad. Sci. U. S. A.* **1976**, *73*, 1078.

[43] S. A. Hollingsworth, D. Batabyal, B. D. Nguyen, T. L. Poulos, *Proc. Natl. Acad. Sci. U. S. A.* **2016**, *113*, 8723.

[44] Y. Hiruma, A. Gupta, A. Kloosterman, C. Olijve, B. Ölmez, M. A. S. Hass, M. Ubbink, *ChemBioChem* **2014**, *15*, 80.

[45] V. Y. Kuznetsov, T. L. Poulos, I. F. Sevrioukova, *Biochemistry* **2006**, *45*, 11934.

Table 1. Monooxygenase activity

PUPPET or Protein mixture	NADH consumption activity ($\times 10^3$ min^{-1})	Coupling efficiency (%)	Monooxygenase activity ($\times 10^3$ nmol min^{-1} (nmol of protein)$^{-1}$)	
			Observed [a]	Calculated [b]
R^1X^1C	1.04 ± 0.02	96.1 ± 1.7	1.00 ± 0.02	0.92
R^2X^1C	1.30 ± 0.01	99.3 ± 1.0	1.29 ± 0.01	1.1
R^3X^1C	1.39 ± 0.02	96.8 ± 0.9	1.35 ± 0.02	1.3 [e]
R^1X^2C	1.35 ± 0.01	99.4 ±0.6	1.34 ± 0.01	1.5
R^2X^2C	1.62 ± 0.01	97.1 ± 1.6	1.57 ± 0.01	1.6
R^3X^2C	1.75 ± 0.01	99.3 ± 1.4	1.74 ± 0.01	1.7
20 nM PdR, 20 nM PdX, 20 nM P450cam	0.005 ± 0.001	*N.D.* [c]	0.005 [d]	-
0.5 μM PdR, 50 μM PdX, 50 nM P450cam (saturated condition)	2.00 ± 0.02	95.2 ± 0.9	1.90 ± 0.02	-

[a]Determined from the NADH consumption activity and the coupling efficiency. [b]Calculated using Eqs. 14 and 16. k_{red}^{RmX1C} and k_{red}^{RmX1} were determined from the V_{max} values of R^mX^1C and R^mX^1, respectively, in cyt*c* reduction assay (Table S5). The turnover number of P450cam determined in saturated conditions (Fig. S9) was used as the value of $k_{cat}^{P450cam}$. [c]Not determined—the consumption amounts of NADH and D-camphor were too low to evaluate the coupling efficiency. [d]Estimated from the NADH consumption rate without reference to coupling efficiency. [e]Estimated using the calculated value of k_{red}^{R3X1C} (Table S5).

Figure legends

Figure 1. Preparation of PUPPETs containing multiple auxiliary proteins. PUPPETs (R^mX^nC) containing multiple copies of PdR and PdX were prepared from a $PCNA1_{G108C}$ fusion protein, a $PCNA2_{L171C}$ fusion protein, and a $PCNA3_{R112C/T180C}$ fusion protein.

Figure 2. Spectral change of P450cam induced by assembly with PdX and PdR. (**A**) UV-vis spectrum of R^1X^1C in the presence of D-camphor (solid line) and a linear combination of the spectra of the component fusion proteins (dotted line). The spectra of the other PUPPETs are shown in Fig. S5. (**B, C**) Difference spectra between free P450cam and P450cam in PUPPETs containing (**B**) one or (**C**) two PdX moieties. The difference spectra of P450cam in PUPPETs containing zero (R^0X^1C and R^0X^2C, red), one (R^1X^1C and R^1X^2C, green), two (R^2X^1C and R^2X^2C, blue) and three PdR moieties (R^3X^1C and R^3X^2C, black) are adjusted by an isosbestic point in the spectra of P450cam (407 nm). (**D, E**) Schematic representation of the transition of binding status of the components in (**D**) R^1X^1C and (**E**) R^1X^2C. (**F**) Plot of the reciprocal of the observed ΔΔAbs against the number of PdR moieties (R^mX^1C, open circle; R^mX^2C, closed circle). To determine the K_2 value, the data for R^mX^1C were fitted to Eq. 1 by using the estimated K_1 and $\Delta\Delta Abs_{max}$ values (solid line). Plots of the reciprocal of the calculated ΔΔAbs for R^mX^2C (m = 1, 2 and 3; Eq. 2) are shown as open squares.

Figure 3. Schematic representation of transition of the binding status of component moieties during the cytochrome *c* reduction process of PUPPET. (**A**) Typical transition of the binding status in R^mX^1C. (**B**) Typical transition of the binding status in R^mX^1C at saturated concentrations of cyt*c*. PdR-bound PdX^{ox} is apparently converted to cyt*c*-bound PdX^{red} (state III to VI) owing to rapid association of PdX^{red} with cyt*c*. (**C**) Typical transition of the binding status in R^mX^2C at saturated concentrations of cyt*c*. R^mX^2C has additional

binding mode: One PdX^{ox} can interact with PdR while the other PdX^{ox} binds to P450cam (state I′ to III′) or PdR (state III to VII).

Figure 4. Schematic representation of transition of the binding status of component moieties during monooxygenation reaction of PUPPET. (**A**) The reaction cycle of $R^{m}X^{1}C$. LS-$P450cam^{3+}$ binds to the substrate accompanied by the dissociation of PdX^{ox} (from state (**1**) to (**2**)). The dissociated PdX^{ox} is reduced (state (**2**) to (**3**)), and then PdX^{red} binds to HS-$P450cam^{3+}$ (state (**3**) to (**4**)). After the first ET and O_2 binding (state (**4**) to (**5**)), the resulting PdX^{ox} dissociates from SO-$P450cam^{3+}$ (state (**5**) to (**6**)) and is then reduced by PdR (state (**6**) to (**7**)). PdX^{red} binds to SO-$P450cam^{3+}$ (state (**7**) to (**8**)) for the second ET, and then the monooxygenation reaction is completed (state (**8**) to (**1**)). (**B**) The reaction cycle of $R^{m}X^{2}C$. After the dissociation of PdX^{ox} (state (**1′**) to (**3**)), HS-$P450cam^{3+}$ binds to PdX^{red} (state (**3**) to (**4**)) for the first ET. HS-$P450cam^{3+}$ is converted to SO-$P450cam^{3+}$ (state (**4**) to (**5**)), and simultaneously the second PdX^{ox} is reduced. After dissociation from PdX^{ox} (state (**5**) to (**7**)), SO-$P450cam^{3+}$ binds to the second PdX^{red} (state (**7**) to (**8**)) for the second ET. Then, the monooxygenase reaction is completed (state (**8**) to (**1**)), and the unbound PdX^{ox} is reduced by PdR (state (**1**) to (**1′**)). (**C**) The proposed reaction cycle of $R^{m}X^{3}C$. After the dissociation of PdX^{ox} (state (**1**) to (**3**)), HS-$P450cam^{3+}$ binds to the first PdX^{red} (state (**3**) to (**4**)). HS-$P450cam^{3+}$ is converted to SO-$P450cam^{3+}$ after the first ET and O_2 binding, and simultaneously the other two PdX^{ox}s in the PUPPET are reduced (state (**4**) to (**5**)). The second PdX^{red} is available for the following second ET (state (**7**) to (**8**)), and the third PdX^{red} is availble for the first ET in the next catalytic cycle.

Figures

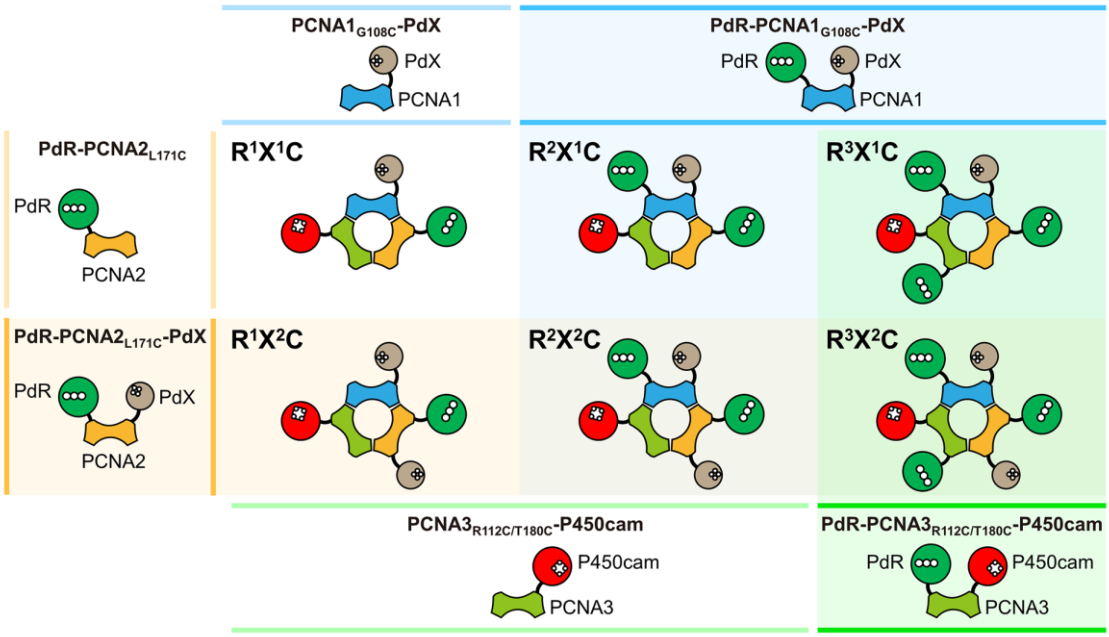

Figure 1.

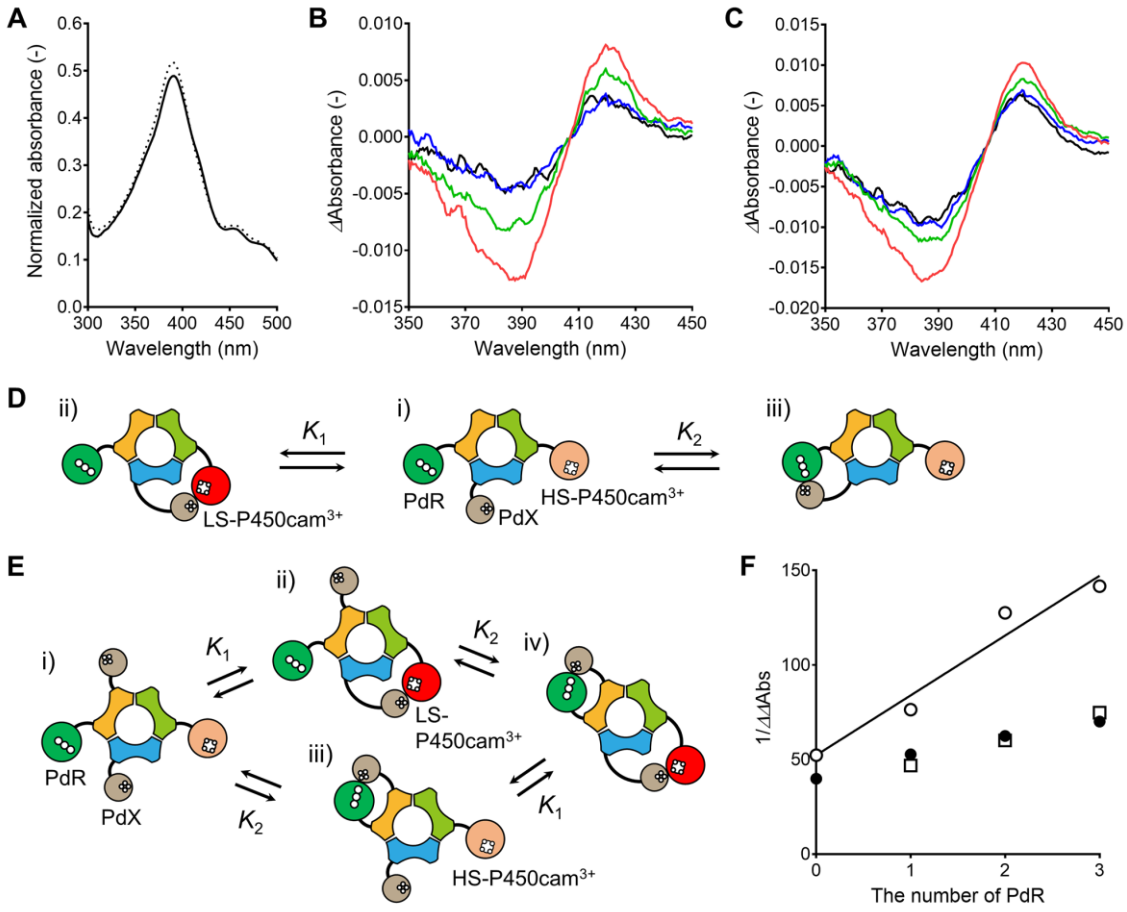

Figure 2.

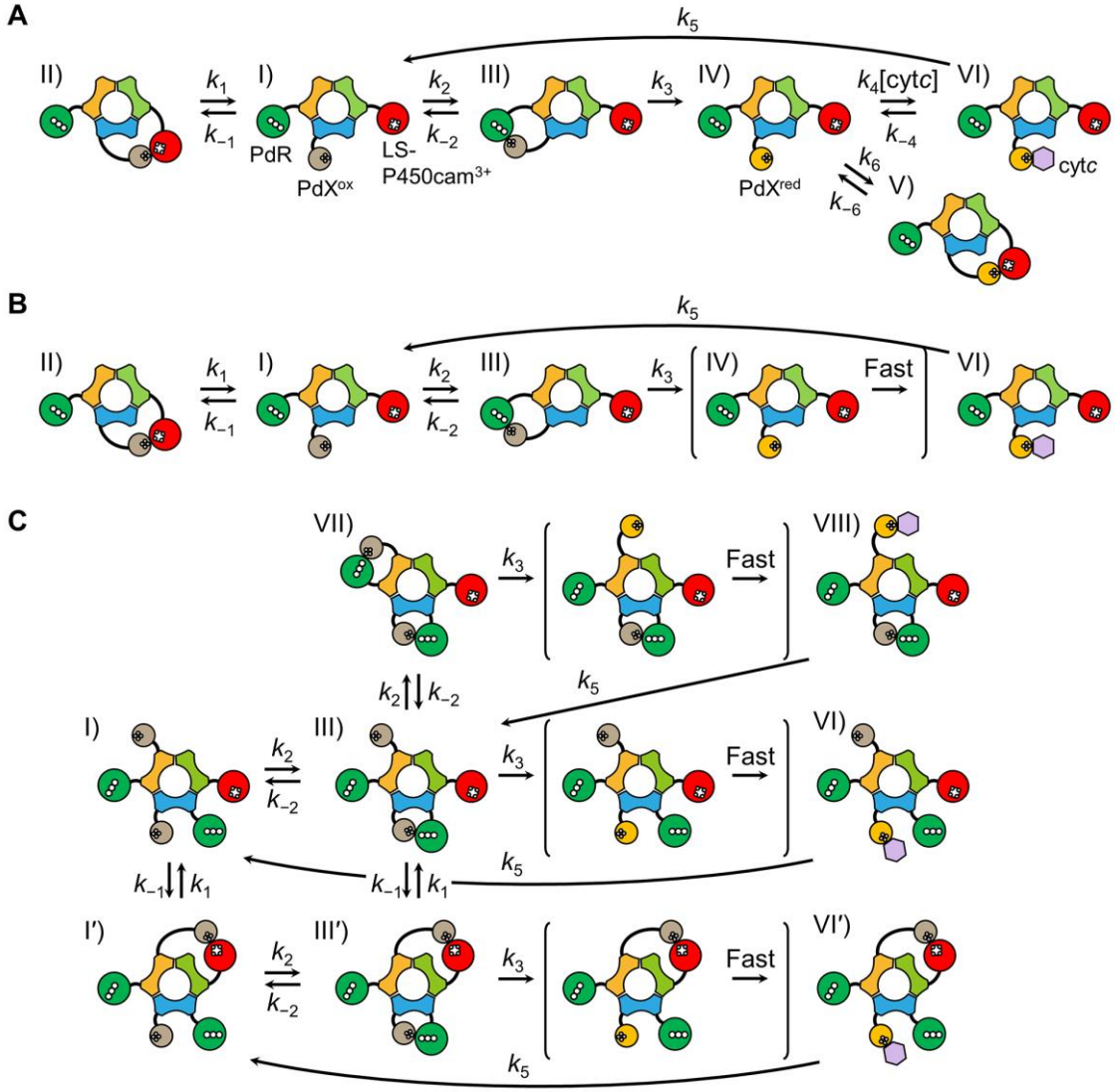
A
II)
I)
III)
IV)
VI)
V)
PdR
PdXox
LS-P450cam3+
PdXred
cytc
k1
k−1
k2
k−2
k3
k4[cytc]
k−4
k5
k6
k−6
B
Fast
C
VII)
VIII)
I′)
III′)
VI′)

Figure 3.

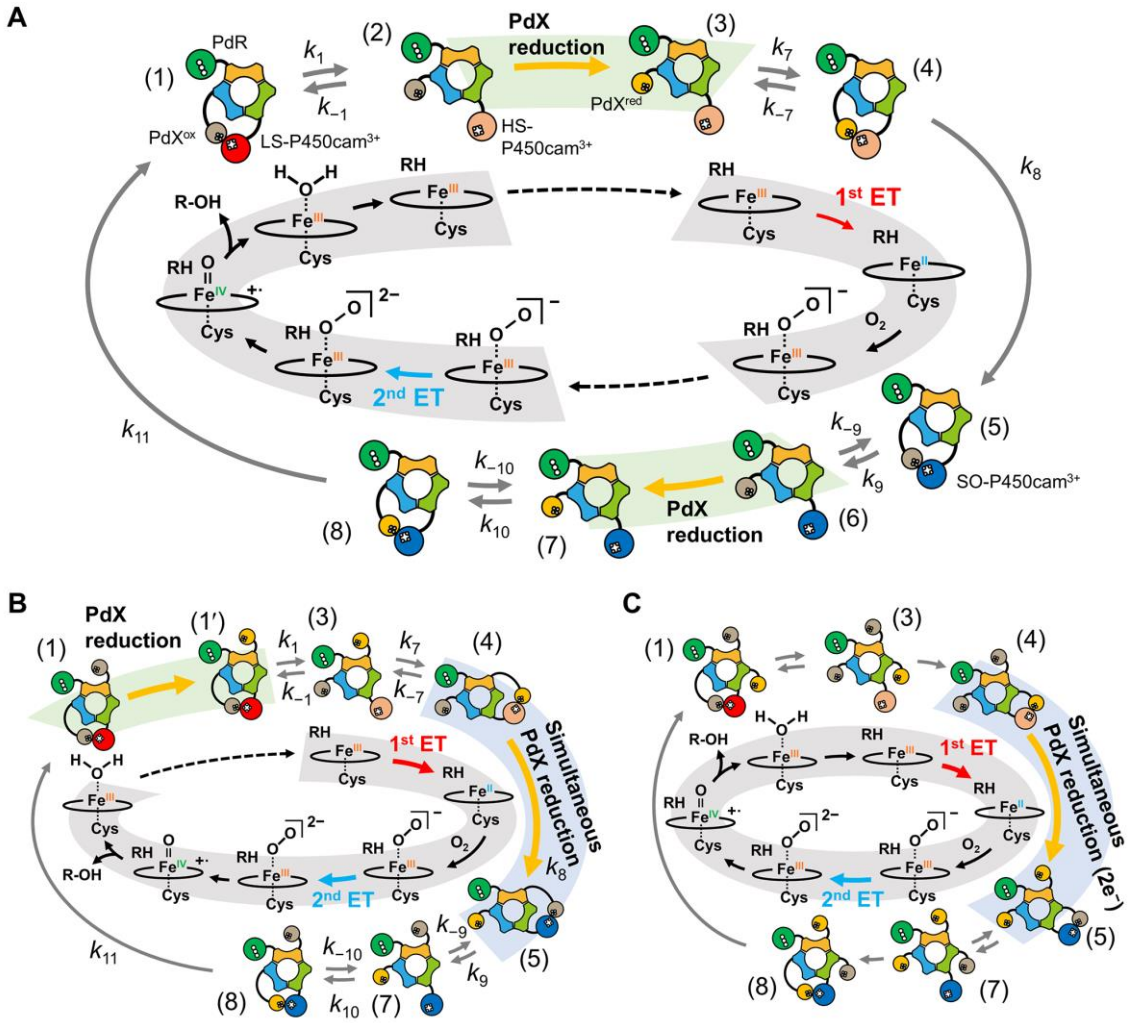
A
PdR
PdX^ox
LS-P450cam3+
PdX reduction
PdX^red
HS-P450cam3+
1st ET
2nd ET
SO-P450cam3+
B
C
Simultaneous PdX reduction
Simultaneous PdX reduction (2e-)

Figure 4.